Numerical Evaluation of the Polarizability Tensors of Stem Cells with Realistic 3D Shapes

Somen Baidya[1], Ahmed M Hassan[1], Beatriz A. Pazmiño Betancourt[2], Jack F. Douglas[2], Edward J. Garboczi[3]
1. Computer Science Electrical Engineering Department, University of Missouri-Kansas City, Kansas City, MO 64110
2. Materials Science and Engineering Division, National Institute of Standards and Technology, Gaithersburg, MD 20899
3. Applied Chemicals and Materials Division, National Institute of Standards and Technology, Boulder, CO 80305

Introduction

Morphological cell analysis has many applications that range from tumorigenesis [1], apoptosis [2], cell division, and proliferation [3]. Therefore, accurate representation and characterization of biological cell shapes has been an area of significant interest over the past few decades [4]. Recent advances in scaffold engineering have enabled researchers to imitate the cell's natural environment *in vitro* [5, 6, 7]. Moreover, advances in imaging technology and segmentation algorithms have facilitated the accurate reconstruction of a cell's three dimensional shape [8, 9, 10]. In this study, we are going to study the electrical properties, specifically the polarizability tensors, of a database of 3D stem cell shapes developed by the National Institute of Standards and Technology (NIST) [11]. The database has the volumetric and surface mesh of 1253 human bone marrow stromal cells (hBMSCs) cultured in ten different microenvironments [12]. The goal of this work is to computationally quantify how variations in cell shape affect their electrical properties.

Theory

Stem cells are undifferentiated cell line that can differentiate into cell of same type or other kind depending on their culturing medium. Culturing the same hBMSCs in ten different biomaterial scaffolds, a group of researchers at NIST were able to obtain a wide range of cell shapes [13, 14]. The cells were then imaged using confocal laser scanning microscopy. After implementing an efficient segmentation algorithm, the cell's 3D shape was presented in *.obj* (wavefront) format and volumetric mesh format (*voxels*) [11]. Based on the material properties of the biomaterial scaffolds, the cell are grouped into ten different cell families, each cell having a unique cell identifier tag [12, 13]. In this study, we computationally studied 50 different cell shapes, 5 from each family, but we are only presenting the results from two cells for brevity [15]. Specifically, we used one cell from the **Porous polystyrene scaffold (PPS)** family and one cell from the **Spuncoat (SC)** family according to the identifiers in Table 1:

Table 1: Cell identifier from the respective family incorporated in this study

Cell Family	Cell Identifier
PPS	012314_SJF_Alvetex_1d_63x_19
SC	082214_SJF_SC_1d_63x_02

The original voxel representation of each cell image is converted into triangular surface mesh representation with five different resolutions: "*down1*", "*down2*", "*down4*", "*down8*", and "*down16*", with "*down1*" being the finest and "*down16*" being the coarsest. Here, we only consider the "*down4*" representation as a good compromise between resolution accuracy and computational time. The considered cell shape listed in table is depicted in Figure 1.

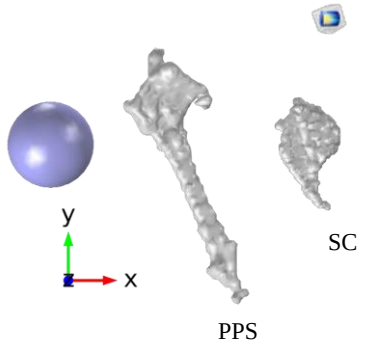

Figure 1. Morphological depiction of the two cell from PPS and SC cell families illustrating the fractal geometry of the shapes. The blue sphere in the left serves as a size scale of 40 μm diameter sphere.

The specific electrical property that we computationally investigate in this study is the electrostatic polarizability of the stem cells. Polarizability is defined as the ratio between the induced dipole moment on a particle and the incident uniform electric field exciting the particle, $p=\alpha E$, where E is the incident electric field, p is the induced dipole moment and α is the polarizability calculated in this work. The polarizability α depends on the shape of the cell, its electrical properties and the electrical properties of its environment. For a spherical cell, α is a scalar quantity, but for a general anisotropic cell α is a tensor:

$$\alpha = \begin{bmatrix} \alpha_{xx} & \alpha_{xy} & \alpha_{xz} \\ \alpha_{yx} & \alpha_{yy} & \alpha_{yz} \\ \alpha_{zx} & \alpha_{zy} & \alpha_{zz} \end{bmatrix} \quad (1)$$

Each element of the polarizability tensor represents the ratio between a specific component of the excited dipole moment and a specific component of the incident field. For example, α_{yz}, represents the ratio between the y component of the induced dipole moment and an incident field oriented in the z-direction. The polarizability tensor in (1) can be diagonalized to yield a matrix with only nonzero diagonal components; P_1, P_2, and P_3; which will be the focus of our work.

Methods

The simplified polarizability expression for a randomly oriented object that can be obtained is (2)

$$\alpha_{ij} = \left(\frac{\epsilon_p}{\epsilon_m} - 1\right) \int_V \hat{\boldsymbol{\imath}} . \boldsymbol{E_j} dV \quad (2)$$

where, i is selectively varied to x, y, and z based on the polarizability element of interest, i is determined by the direction of the incident field, and V is the volume of the inclusion. The field direction j is similarly varied to obtain the nine element matrix. ϵ_p corresponds to the relative permittivity of the particle and ϵ_m denotes the relative permittivity of the surrounding medium set to unity in this work. For a perfect electric conductor (i.e $\epsilon_p = \infty$) the integral will correspond to electric polarizability (α_E) and for a perfect magnetic conductor ($\epsilon_p = 0$) the integral will represent the magnetic polarizability (α_M) of the particle [16]. For an arbitrary value of ϵ_p, the general polarizability tensor can be calculated.

The electric field in (2) can be obtained by the solution of the electrostatic Laplace equation throughout the computational domain using the Electrostatics physics interface under the AC/DC COMSOL® module [17].

The *.obj* formatted surface mesh of each cell obtained from the NIST database is converted into *STL* (STereoLithography) format using MeshLab [18] to facilitate the import operation to COMSOL®. The cell shape of interest is then enclosed by a bounding sphere, the radius of which was at least 25 times larger than the size of the cell imported, to replicate free space conditions. The entire computational domain is the re-meshed into small volumetric tetrahedrals. Due to fractal geometry of the imported cell surfaces, we performed a "*Composite Face*" formation under "*Virtual Operation*" to represent the cell as a single entity. The relative permittivity of the cell's bounding medium was set to unity, $\epsilon_m = 1$, and the imported cell was assigned a variable permittivity depending on the polarizability (electric/ magnetic) of interest. Under the Electrostatic physics, we used "*Electric Displacement Field*" excitation on the bounding sphere and assigned an arbitrary point in the domain as a reference ground for better convergence. To validate the COMSOL® results we compared them to those obtained using the open-source Scuff-EM (Surface CUrrent/Field Formulation of ElectroMagnetism) method which is based on the independent Boundary Element Method (BEM) [19].

Results

To illustrate the importance of meshing, we present Figure 2 where the electric polarizability values calculated using COMSOL® are depicted with respect to the inverse of the number of tetrahedral elements used. The theoretical value of the volume normalized polarizability of a sphere is 3 [20, 21]. As shown in Figure 2, as $N \longrightarrow \infty$ (i.e N^{-1} approaches zero), the calculated value converges to the theoretical value of 3. To optimize the computational time and resource as well as achieve better accuracy in our calculations, we performed the simulations at two different resolutions and used linear extrapolation to yield more accurate polarizability values.

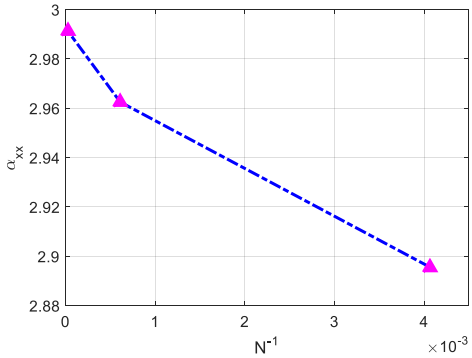

Figure 2. Convergence plot of COMSOL® result as the Number of tetrahedral elements approaches ∞

The computed Electric and Magnetic polarizability values obtained are listed in Table 2 and Table 3, respectively. All polarizability values reported in this study are normalized by the volume of respective cell.

Table 2: Diagonalized Electric Polarizability comparison of "*down4*" mesh representation of the two cells[1] between Scuff-EM and COMSOL®.

Cell Family	α_E	COMSOL®	Scuff-EM	Percentage Uncertainty
PPS	P_1	44.450	47.9470	7.29%
	P_2	4.4613	4.6767	4.61%
	P_3	2.2693	2.3609	3.88%
SC	P_1	10.1200	10.6230	4.74%
	P_2	4.3223	4.4926	3.79%
	P_3	2.0335	2.1155	3.88%

The polarizability tensors are marked in a descending order, i.e. $P_1>P_2>P_3$. The level of agreement between the results further solidifies the accuracy of our calculation and implementation of the desired physics in respective solver.

For electric polarizability (α_E), the extrapolation was obtained from two different meshing resolution. We have summarized the number of elements and respective computational time[2] required for each cell polarizability calculation in Table 4.

Figure 3(a) and 3(b) highlights the successful implementation of *Padé* approximation in the calculation of intrinsic conductivity for both of the cells [22]. We performed a parametric sweep on the contrast of the cells to compare the intrinsic conductivity with the *Padé* approximation, each of which took 4 hours to complete.; whereas the *Padé* approximation required no time at all given that we already know the $[\sigma]_0$ and $[\sigma]_\infty$ for respective cells.

Table 4: Diagonalized Magnetic Polarizability comparison of "*down4*" mesh representation between Scuff-EM and COMSOL®.

Cell Family	α_M	COMSOL®	Scuff-EM	Percentage Uncertainty
PPS	M_1	2.356	2.286	3.05%
	M_2	1.658	1.648	0.62%
	M_3	1.255	1.280	1.92%
SC	M_1	2.393	2.297	4.19%
	M_2	1.495	1.460	2.41%
	M_3	1.284	1.274	0.79%

Conclusions

The significance of this study lies in the level of agreement between different solvers in polarizability calculation and successful implementation of *Padé* approximation of any object of arbitrary shape. We believe that, the findings of the study will help interested group to work with any biological or non-biological objects' characteristics evaluation. In

Table 3: Parametric Comparison between COMSOL® and Scuff-EM solver

Cell Family	Meshing Resolution	Number of Elements		Volume		Computational Time[2] (Minutes)	
		COMSOL® (Tetrahedral)	Scuff-EM (Face)	COMSOL®	Scuff-EM	COMSOL®	Scuff-EM
PPS	Normal	193727	5748	14869.69704	14877.1445	10.6	0.87
	Refined	1300369	22992	14874.71191	14877.1689	21.35	49.18
SC	Normal	503895	10632	8234.823461	8235.94531	12.7	4.58
	Refined	2523392	42528	8235.632796	8235.94141	30.65	317.2

[1] Each family name corresponds to the cell morphology listed in Table 1.

[2] All computational times were measured on an Intel Xeon Processor E5-2687W with 20 MB Cache and 3.10 GHz processor base frequency. The values in the table only shows the run time of each solver. An additional ~ 1 hour was needed to adapt the format of each cell to formats that are compatible with each solver.

future, we want to keep adding more shapes in our dataset and help the existing literature better understand the effect of shape variation in electrical characterization and their interpretation.

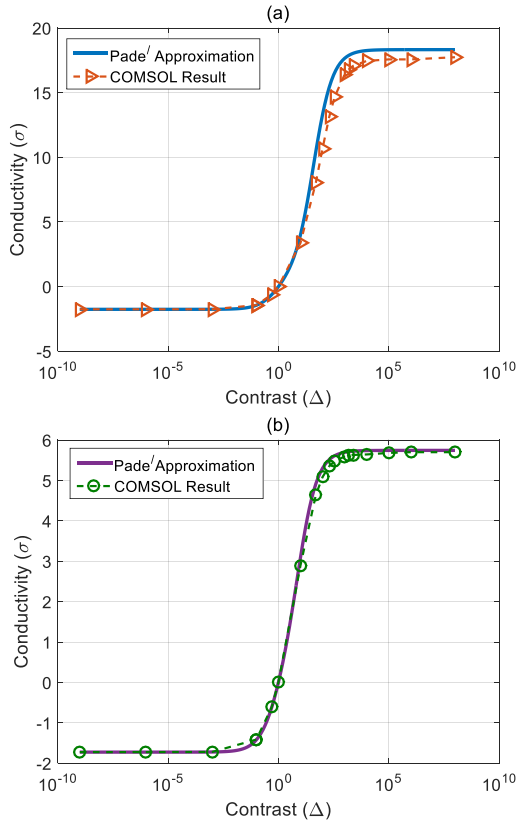

Figure 3. Padé approximation validation in comparison to COMSOL® "*down4*" results obtained for 20 different values of Δ illustrated for the case of two families (a) PPS and (b) SC

References

[1] T. Xie, M. Zeidel and Y. Pan, "Detection of tumorigenesis in urinary bladder with optical coherence tomography: optical characterization of morphological changes," *Optics Express*, vol. 10, no. 24, p. 1431, 2002.

[2] G. A. Losa and C. Castelli, "Nuclear patterns of human breast cancer cells during apoptosis: characterisation by fractal dimension and co-occurrence matrix statistics," *Cell and Tissue Research*, vol. 322, no. 2, pp. 257-267, 2005.

[3] M. Colombi, L. Moro, N. Zoppi and S. Barlati, "Quantitative Evaluation of mRNAs byIn SituHybridization and Image Analysis: Principles and Applications," *DNA and Cell Biology*, vol. 12, no. 7, pp. 629-636, 1993.

[4] E. C. Jensen, "Overview of Live-Cell Imaging: Requirements and Methods Used," *The Anatomical Record: Advances in Integrative Anatomy and Evolutionary Biology*, vol. 296, no. 1, pp. 1-8, 2012.

[5] S. Liao, L. T. Nguyen, M. Ngiam, C. Wang, Z. Cheng, C. K. Chan and S. Ramakrishna, "Biomimetic nanocomposites to control osteogenic differentiation of human mesenchymal stem cells," *Advanced healthcare materials*, vol. 3, no. 5, pp. 737-751, 2014.

[6] S. J. Florczyk, M. Leung, Z. Li, J. I. Huang, R. A. Hopper and M. Zhang, "Evaluation of three-dimensional porous chitosan--alginate scaffolds in rat calvarial defects for bone regeneration applications," *Journal of Biomedical Materials Research Part A*, vol. 101, no. 10, pp. 2974-2983, 2013.

[7] K. Chatterjee, S. Lin-Gibson, W. E. Wallace, S. H. Parekh, Y. J. Lee, M. T. Cicerone, M. F. Young and C. G. Simon, "The effect of 3D hydrogel scaffold modulus on osteoblast differentiation and mineralization revealed by combinatorial screening," *Biomaterials*, vol. 31, no. 19, pp. 5051-5062, 2010.

[8] P. a. S. M. Bajcsy, S. Florczyk, C. Simon, D. Juba and M. Brady, "A method for the evaluation of thousands of automated 3D stem cell segmentations," *Journal of Microscopy*, vol. 260, no. 3, pp. 363-376, 2015.

[9] P. Bajcsy, A. Cardone, J. Chalfoun, M. Halter, D. Juba, M. Kociolek, M. Majurski, A. Peskin, C. Simon, M. Simon, A. Vandecreme and M. Brady, "Survey statistics of automated segmentations applied to optical imaging of mammalian cells," *BMC Bioinformatics*, vol. 16, no. 1, p. 330, 2015.

[10] G. Pucihar, T. Kotnik, B. Valič and D. Miklavčič, "Numerical Determination of Transmembrane Voltage Induced on Irregularly Shaped Cells," *Annals of Biomedical Engineering*, vol. 34, no. 4, pp. 642-652, 2006.

[11] "NIST Computational Science in Metrology," National Institute of Standards and Technology, 2017. [Online]. Available: https://isg.nist.gov/deepzoomweb/fileBrowsing/3D/.

[12] S. Florczyk, M. Simon, D. Juba, S. Pine, S. Sarkar, D. Chen, P. Baker, S. Bodhak, A. Cardone, M. Brady and others, "A Bioinformatics 3D Cellular Morphotyping Strategy for Assessing Biomaterial Scaffold Niches," *ACS Biomaterials Science &*

Engineering, vol. 3, no. 10, pp. 2302-2313, 2017.

[13] B. P. Betancourt, S. Florczyk, M. Simon, D. Juba, J. F. Douglas, W. Keyrouz, P. Bajcsy, C. Lee and C. G. Simon, "Effect of the Scaffold Microenvironment on Cell Polarizability and Capacitance Determined by Probabilistic Computations," *Biomedical Materials*, vol. 13, no. 2, p. 025012, 2018.

[14] T. M. Farooque, C. H. Camp, C. K. Tison, G. Kumar, S. H. Parekh and C. G. Simon, "Measuring stem cell dimensionality in tissue scaffolds," *Biomaterials*, vol. 35, no. 9, pp. 2558-2567, 2014.

[15] S. Baidya, A. M. Hassan, B. A. P. Betancourt, J. F. Douglas and E. J. Garboczi, "Analysis of Different Computational Techniques for Calculating the Polarizability Tensors of Stem Cells with Realistic Three-Dimensional Morphologies," *IEEE Transactions on Biomedical Engineering*, Under Review.

[16] F. Vargas Lara, A. M. Hassan, E. J. Garboczi and J. F. Douglas, "Intrinsic conductivity of carbon nanotubes and graphene sheets having a realistic geometry," *The Journal of Chemical Physics*, vol. 143, no. 20, p. 204902, 2015.

[17] "COMSOL Multiphysics v. 5.2," *COMSOL AB, Stockholm, Sweden*, 2015.

[18] P. Cignoni, M. Callieri, M. Corsini, M. Dellepiane, F. Ganovelli and G. Ranzuglia, "MeshLab: an Open-Source Mesh Processing Tool," in *Eurographics Italian Chapter Conference*, The Eurographics Association, 2008, pp. 129-136.

[19] M. H. Reid and S. G. Johnson, "Efficient Computation of Power, Force, and Torque in BEM Scattering Calculations," *IEEE Transactions on Antennas and Propagation*, vol. 63, no. 8, pp. 3588-3598, 2015.

[20] A. Sihvola, P. Yla-Oijala, S. Jarvenpaa and J. Avelin, "Polarizabilities of platonic solids," *IEEE Transactions on Antennas and Propagation*, vol. 52, no. 9, pp. 2226-2233, 2004.

[21] A. H. Sihvola, "Electromagnetic Mixing Foormulas and Applications," in *Electromagnetic Wave Series*, 47 ed., London: IEEE, 1999.

[22] E. Garboczi and J. Douglas, "Intrinsic conductivity of objects having arbitrary shape and conductivity," *Physical Review E*, vol. 53, no. 6, p. 6169, 1996.

Acknowledgements

This work was supported in part by the NIST Grant 70NANB15H28 and by the University of Missouri-Kansas City, School of Graduate Studies Research Award.